Volume 1 | Number 1 | Jan 2013 | Pages 1–100

Journal of
Materials Chemistry A

Materials for energy and sustainability
www.rsc.org/materialsA

Li⁺

ROYAL SOCIETY
OF CHEMISTRY

ROYAL SOCIETY
OF CHEMISTRY

www.rsc.org/materialsA

Journal Name

ARTICLE

Graphene Aerogel Prepared by Thermal Evaporation of Graphene Oxide Suspension Containing Sodium Bicarbonate

Shaolin Yang,[ab] Li Zhang,[a] Qiuyun Yang,[a] Zihan Zhang,[a] Bo Chen,[a] Peng Lv,[a] Wei Zhu*[a] and Guanzhong Wang*[a]

We present a facile, environment-friendly and mild method to fabricate graphene hydrogel by heating graphene oxide (GO) suspension containing sodium bicarbonate (NaHCO$_3$). This method demonstrates a new type of *in situ* reduction-assembly approach to construct graphene hydrogel through simultaneous water evaporation and GO reduction. The freeze-dried graphene aerogel (G-Gel) shows excellent adsorptivity to heavy metal ions and dyes. The thermally treated G-Gel (TG-Gel) exhibits promising performance in recyclable selective absorption of oil and organic solvents.

Introduction

Since the discovery of the first isolated graphene layer from mechanical cleavage of bulk graphite,[1] graphene, a two dimensional carbon monolayer, has attracted extensive attention owing to its remarkable electrical, mechanical, chemical, thermal and optical properties.[2-9] These extraordinary properties endow graphene with a variety of potential applications including nanoelectronic[10] and photonic devices,[11, 12] energy conversion and storage,[13, 14] environmental remediation,[15] catalysis,[16, 17] sensors,[18, 19] composite materials[20] and biotechnology.[21, 22] However, these applications are usually significantly compromised by the π-π interactions and van der Waals forces among individual graphene sheets being assembled into macroscopic objects, which cause those sheets to restack and self-aggregate, leading to a decrease in the accessible surface area. In order to overcome this obstacle, three-dimensional (3D) graphene architectures such as hydrogels, aerogels, and macroporous films have been developed.[14, 23-27] These novel materials usually exhibit large specific surface areas, light weight, strong mechanical strength, and good electrical and thermal conductivity.

Among fabrication strategies of 3D graphene architectures such as template assembly,[28-30] template-directed chemical vapor deposition,[31, 32] flow-directed self-assembly[33, 34] and cross-linking,[35-37] *in situ* reduction-assembly of graphene oxide[38-41] seems to be the most preferable one thanks to its unique advantages such as facile procedure and easy scalability. Previously, *in situ* reduction-assembly has been realized by reduction under extreme hydrothermal conditions of high pressure and temperature[40, 42] or with chemical agents that are usually toxic.[39, 43-47]

Herein we demonstrate a new type of *in situ* reduction-assembly method to prepare graphene hydrogel through the combined water thermal evaporation and GO reduction process. Gelation was accomplished by heating the mixed solution of GO and NaHCO$_3$ at 100 °C, representing a green and mild method. We believe that generated bubbles prevented the restacking of the self-assembled reduced graphene oxide (rGO) and thus resulted in the formation of graphene hydrogel. The hydrophilic graphene aerogel (G-Gel) obtained by freeze-drying of the as-prepared graphene hydrogel exhibit great adsorption ability to heavy metal ions and dyes. The hydrophobic TG-Gel made by thermal treatment of G-Gel gave excellent performance in repeatable selective absorption of oil and organic solvents.

Experimental

Materials

Natural graphite flake (-325 mesh, 99.8%) was purchased from Alfa Aesar and used for synthesizing graphene oxide. Sulfuric acid (H$_2$SO$_4$, 98%), hydrochloric acid (HCl, 36%), potassium permanganate (KMnO$_4$, 99.5%), sodium nitrate (NaNO$_3$, 99%), hydrogen peroxide (H$_2$O$_2$, 30%), sodium bicarbonate (NaHCO$_3$, 99.5%), potassium bicarbonate (KHCO$_3$, 99.5%), ammonium bicarbonate (NH$_4$HCO$_3$, analytical reagent), ammonium carbonate ((NH$_4$)$_2$CO$_3$, analytical reagent), potassium chloride (KCl, 99.5%), sodium chloride (NaCl, 99.5%), sodium hydroxide (NaOH, 96%), chloroplatinic acid hexahydrate (H$_2$PtCl$_6$·6H$_2$O, analytical reagent), chloroauric

acid hydrate ($HAuCl_4 \cdot 4H_2O$, analytical reagent), lead nitrate ($Pb(NO_3)_2$, 99%), cadmium sulfate 8/3-hydrate ($CdSO_4 \cdot 8/3H_2O$, 99%), silver nitrate ($AgNO_3$, 99.8%), Cupric nitrate ($Cu(NO_3)_2$, 99.8%), various dyes and organic solvents were purchased from Sinopharm Chemical Reagent Co., Ltd., China. Sodium Carbonate (Na_2CO_3, 99.8%) was bought from Shanghai Lingfeng Chemical Reagent Co., Ltd., China.

Preparation of G-Gel and TG-Gel

Graphene oxide was prepared by the oxidation of natural graphite flake according to Hummers' method.[48] The mixed solution of 5 mL GO (previously ultra-sonicated for 60 min) and 0.1 g $NaHCO_3$ in an open beaker was heated in a water bath at 100 °C without stirring. Upon heating, the color of the solution gradually changed from brown to black. Meanwhile, with evaporation of water, a thick gel-like membrane formed at the air-liquid interface after several minutes. This hydrogel membrane grew in thickness with continuous heating and the solution was finally transformed into hydrogel monolith. Then, 10 mL of hot NaCl solution was added, and the beaker was continuing heated at 90 °C for 30 minutes. After that, the hydrogel was transferred to a vessel filled with distilled water and shaken on a multifunctional shaker for 2 days to remove excessive reactants. During this period, the distilled water was renewed every 5 h. The G-Gel was obtained after freeze-drying of the graphene hydrogel. Thermal annealing of the G-Gel at 800 °C for 1 hour under the flowing stream of argon gave a hydrophobic TG-Gel.

Characterization

Scanning electron micrographs (SEM) were performed on a field-emission scanning electron microscope (JSM-6700F, JEOL, Japan), Raman spectra were carried out on a micro-Raman microscope (Horiba JobinYvon LabRAM HR-800) using 514 nm laser, X-ray photoelectron spectroscopy (XPS) was performed on an ESCALAB 250Xi X-ray Photoelectron Spectrometer, X-ray diffraction (XRD) analysis was recorded in a Rigaku RINT-TTR III X-ray Diffractometer, and Fourier transform infrared (FTIR) spectra were measured using a Nicolet 8700 FT-IR spectrometer (Thermo Scientific) in the range of 4000-500 cm^{-1}.

Heavy metal ions adsorption

The G-Gel was immersed into a hermetic vessel containing 20 mL of heavy metal ion solution with concentration of 200 mg L^{-1}. After 5 days, the G-Gel was removed and the concentration of the metal ion was measured using inductively coupled plasma-atomic emission spectroscopy (ICP-AES, Optima 7300DV, PerkinElmer, USA). The adsorption capacity (Q_m) of the heavy metal ion with the G-Gel was calculated by $Q_m = (C_i - C_f)V/m$, where C_i and C_f are the initial and final liquid-phase concentrations of the heavy metal ions (mg L^{-1}), respectively, while V is the volume of the heavy metal ions solution (L) and m is the mass of the G-Gel used (g).

Adsorption of dyes

All dye adsorption experiments were carried out at room temperature to test the adsorption capacities of dyes with G-Gel. In a typical experiment, the G-Gel was placed into 20 mL aqueous solution containing dye with concentration of 400 mg L^{-1}. After the adsorption reached equilibrium, the G-Gel was removed from the solution, and the dye concentration was determined by UV-vis adsorption spectroscopy. The amount of dye adsorbed on per unit mass of G-Gel was calculated according to the equation of $Q_d = (C_o - C_e)V/m$. Here, C_o and C_e are respectively the initial and equilibrium concentrations of the dye solution (mg L^{-1}), V is the volume of dye solution (L) and m is the weight of G-Gel (g).

Absorption of organic liquids

The TG-Gel was putted into organic liquid which is floating on the water. After the absorption was done, the TG-Gel was removed. Before and after absorbing organic liquids, the TG-Gels were weighed with a balance (Mettler Toledo AL104). The rate of weight gain (Q_o) of TG-Gel after absorption of organic solvents was obtained using the equation $Q_o = (M_a - M_b)/M_b$, where M_a and M_b are the weights of TG-Gel after and before absorption.

Results and discussion

In a typical procedure, to an open beaker was added a mixture of 0.1 g of $NaHCO_3$ and 5 mL of GO suspension (4 g L^{-1}). The mixed solution was heated in a water bath at 100 °C without stirring. Upon heating, the color of the solution gradually changed from brown to black and a thick hydrogel membrane formed at the liquid surface after several minutes. This hydrogel membrane grew in thickness with evaporation of water and the solution was finally condensed to hydrogel monolith. 10 mL of hot NaCl solution was then slowly added and the beaker was heated at 90 °C for an extra 30 minutes for purpose of stabilizing the as-prepared graphene hydrogel. The graphene hydrogel monolith was then floating on the top of the NaCl solution (Fig. 1A). Freeze-drying of the hydrogel gave 14.2 mg of graphene aerogel (G-Gel) (Fig. 1B), which supported a weight of 100 g without obvious deformation (Fig. 1C).

Fig. 1D shows the complete permeation of the G-Gel by one drop of water, indicating the hydrophilic characteristic of the G-Gel. However, it became hydrophobic (TG-Gel, Fig. 1E) after being treated with thermal annealing at 800 °C in argon atmosphere for 1 hour. This change could be attributed to the decrease of polar functionalities on the surface upon thermal annealing.[49]

Fig. 2A shows the C 1s XPS spectra of GO, G-Gel and TG-Gel. The spectrum of GO is featured by the peaks at 284.3, 286.4 and 287.8 eV respectively corresponding to C-C, C-O and C=O bonds.[50] The G-Gel spectrum has a more prominent C-C peak (284.8 eV) and much weaker C-O and C=O peaks, suggesting the removal of most oxygenated groups of GO through reduction with $NaHCO_3$ during gelation. The peaks associated with oxygenated groups were further weakened in the spectrum of TG-Gel, indicating that the G-Gel was reduced to a higher extent upon thermal annealing process.
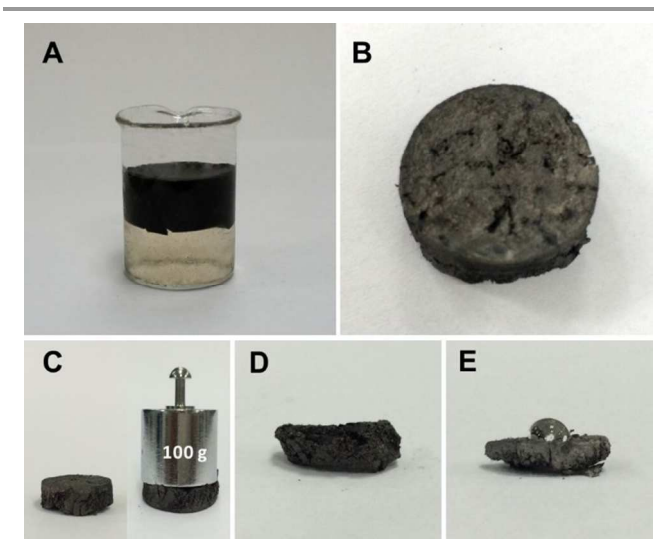
Fig. 1 Photographs of as-prepared graphene hydrogel (A), freeze-dried G-Gel (B), a G-Gel supporting 100 g weight (C), and water dripped on G-Gel (D) and TG-Gel (E).

The Raman spectra of GO, G-Gel and TG-Gel show two strong G and D bands at the vicinity of 1590 and 1350 cm⁻¹

(Fig. 2B), which could be ascribed to graphitic domains and structural defects, respectively. The intensity ratio of D/G bands for GO of 0.88 increased to 0.96 for G-Gel, and further to 1.13 for TG-Gel. These increments suggest decreases in the average sp^2 domain size upon chemical reduction and thermal annealing, which probably be ascribable to the formation of large amounts of new smaller graphitic domains.[49]

The XRD patterns of GO, G-Gel and TG-Gel are depicted in Fig. 2C. The featured diffraction peak of GO appears at 11.65°, corresponding to an interlayer spacing distance of 0.759 nm, which is much larger than that of pristine graphite (0.335 nm). This difference probably originated from the grafting of oxygen-containing functional groups of GO.[51] Instead of the GO peak, a broad peak appears at near 21.92° for G-Gel, indicating that the interlayer spacing of G-Gel had reduced to 0.405 nm by virtue of the removal of the functional groups. The interlayer distance further reduced to 0.345 nm (2θ=25.80°) for TG-Gel, suggesting the further removal of the oxygenated functional groups through the thermal annealing process. Moreover, the expanded weak peaks of G-Gel and TG-Gel could be ascribed to the formation of structurally defected graphene sheets in smaller sizes as well as the turbostratic arrangement of the few-layer stacked sheets.[52, 53]
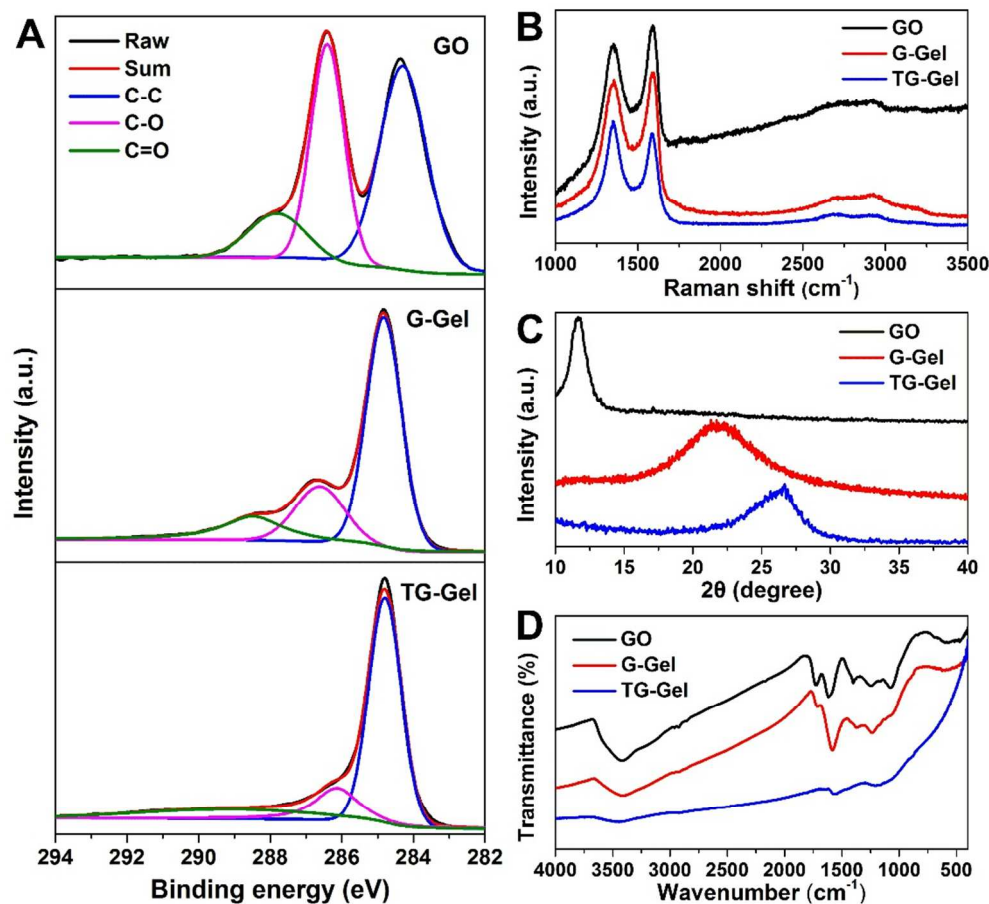

Fig. 2 Characterizations of the chemical structure of GO, G-Gel and TG-Gel: (A) C 1s XPS spectra; (B) Raman spectra; (C) XRD patterns; (D) FTIR spectra.

The reductions of oxygen-containing groups in GO were also confirmed by FTIR spectroscopy, as shown in Fig. 2D, where FTIR spectra of GO, G-Gel and TG-Gel were compared. The spectrum of GO exhibits the presence of plenty of oxygen

functional groups, such as the strong and broad peaks around 3419 and 1400 cm^{-1} ascribable to hydroxyl groups, the peak at 1725 cm^{-1} attributable to carbonyl groups, and the peaks at 1242 and 1075 cm^{-1} assignable to C-O bonds. The band at 1617 cm^{-1} is associated with aromatic C-C stretching vibration of graphitic domains.[54] As for G-Gel, the absorption bands of these oxygenated groups weakened, suggesting that to some extent the GO was reduced. The thermal treatment of G-Gel resulted in a drastic decrease or disappearance of the peaks assigned to these oxide groups on TG-Gel, indicating that most oxygen-containing functional groups were further removed.

The scanning electron microscopic (SEM) image of the G-Gel shows an interconnected 3D porous structure (Fig. 3A). The pores of the 3D network sized at tens of micrometers are bounded by walls consisting thin layers of stacked graphene sheets. The partial overlapping of graphene sheets resulted in the formation of physical cross-linking sites of framework of the graphene hydrogel. The wrinkled and folded morphology is also observed on the surfaces of the assembled graphene sheets (Fig. 3B).
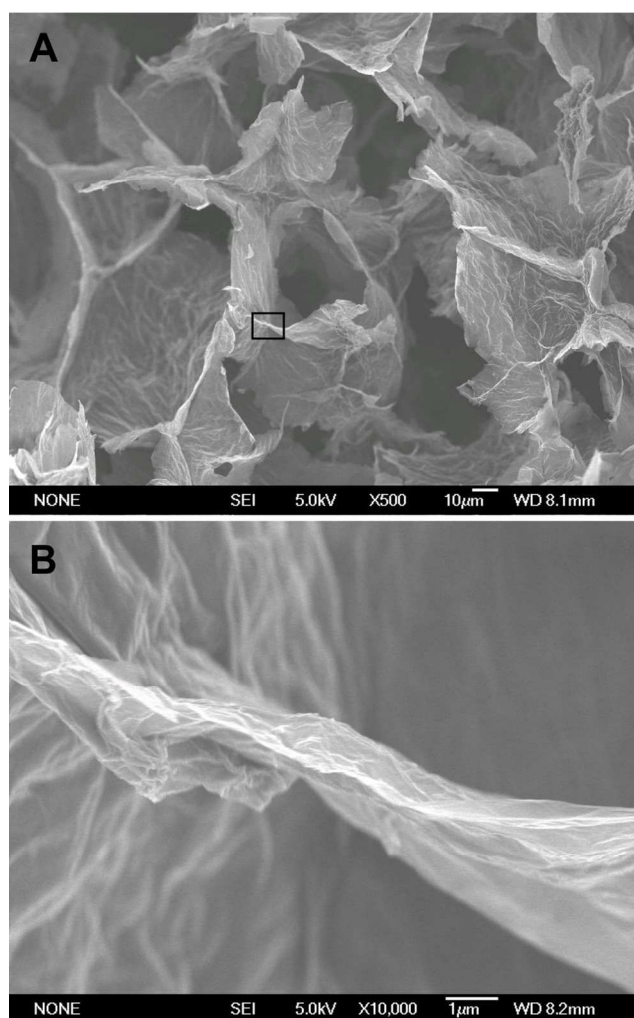

Fig. 3 SEM images of the G-Gel. (B) is the magnification of the square in (A).

To study the influence of GO concentration on the derived G-Gel, we prepared G-Gels with the GO concentration varied from 1 to 5 mg mL^{-1}. The SEM images of G-Gels obtained under different GO concentrations exhibit 3D porous architectures without obvious morphology difference among one another (Fig. 4). All concentrations gave volume per unit mass (1/ρ) values around 130 cm^3 g^{-1} (Fig. 5). It seems that the graphene hydrogel does not form until enough water has been evaporated to reach an enough high GO concentration.
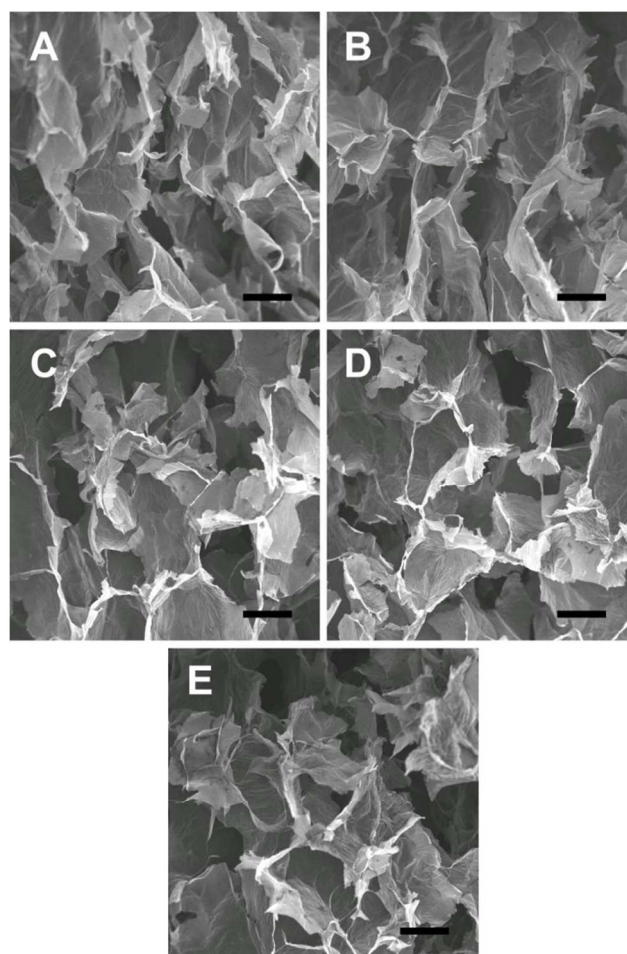

Fig. 4 SEM images of G-Gels prepared by different GO concentrations. (A) 1 mg mL^{-1}, (B) 2 mg mL^{-1}, (C) 3 mg mL^{-1}, (D) 4 mg mL^{-1} and (E) 5 mg mL^{-1}. Scale bar: 50 μm.
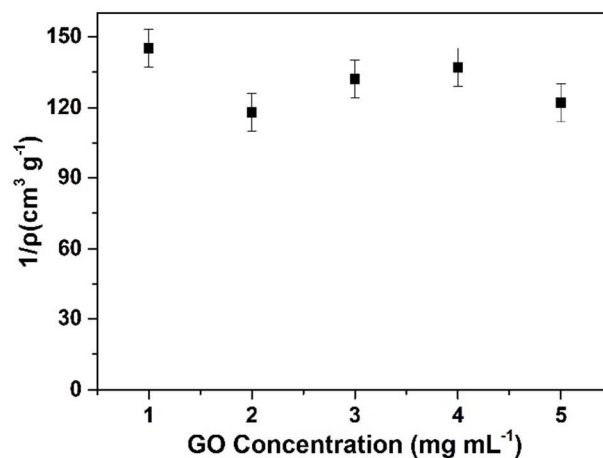
Fig. 5 The volume per unit mass ($1/\rho$) of the G-Gel prepared from different GO concentrations.

In order to investigate the mechanism of graphene hydrogel formation, other reactants were used to replace $NaHCO_3$ for preparation of G-Gel (Table 1). For all reactants except NaCl, the GO suspension turned black when it reacted with the compound under heating, indicating the reduction of GO. This probably be attributed to the alkaline medium caused by dissolution of the reactant.[55] However, only $NaHCO_3$, NH_4HCO_3 and $(NH_4)_2CO_3$ resulted in gelation of rGO. In addition, bubbles were generated in reactions using these three compounds, probably due to heat-promoted decomposition. To determine the role of bubbles in hydrogel formation, these compounds were further investigated with different amounts. Based on the membrane formation and gelation conditions shown in Table 2, we propose that reduction of GO by these compounds is simultaneous with self-assembly of rGO at the liquid-air interface during evaporation of water upon heating. As schematic drawings shown in Fig. 6, the restacking of rGO is prevented by the bubbles generated in this process so the hydrogel membrane could form. An appropriate amount of bubbles is important for rGO gelation, excessive bubbles would destroy the self-assembly of membrane, and too few would not impede the restacking of rGO effectively to avoid merely thin membrane formation.

The formed graphene hydrogel seemed susceptible to fragmentation when being soaked in water for a long time. However, the hydrogel could be stabilized by heating in salt solution such as NaCl or KCl for tens of minutes probably by

virtue of the salt-out effect. As shown in the inset in Fig. 6, salt ions attract water molecules at corners of cross-linking sites formed by partially overlapped graphene sheets, leading to larger overlapped area at cross-linking sites and consequently more stable framework of the graphene hydrogel.

Table 1 Color change and gelation of GO with different reactants.

Reactant	Turn black	Gelation
$NaHCO_3$	√	√
$KHCO_3$	√	×
NH_4HCO_3	√	√
Na_2CO_3	√	×
NaOH	√	×
NaCl	×	×
$(NH_4)_2CO_3$	√	√

Table 2 Membrane formation and gelation of rGO with different amounts of reactants.

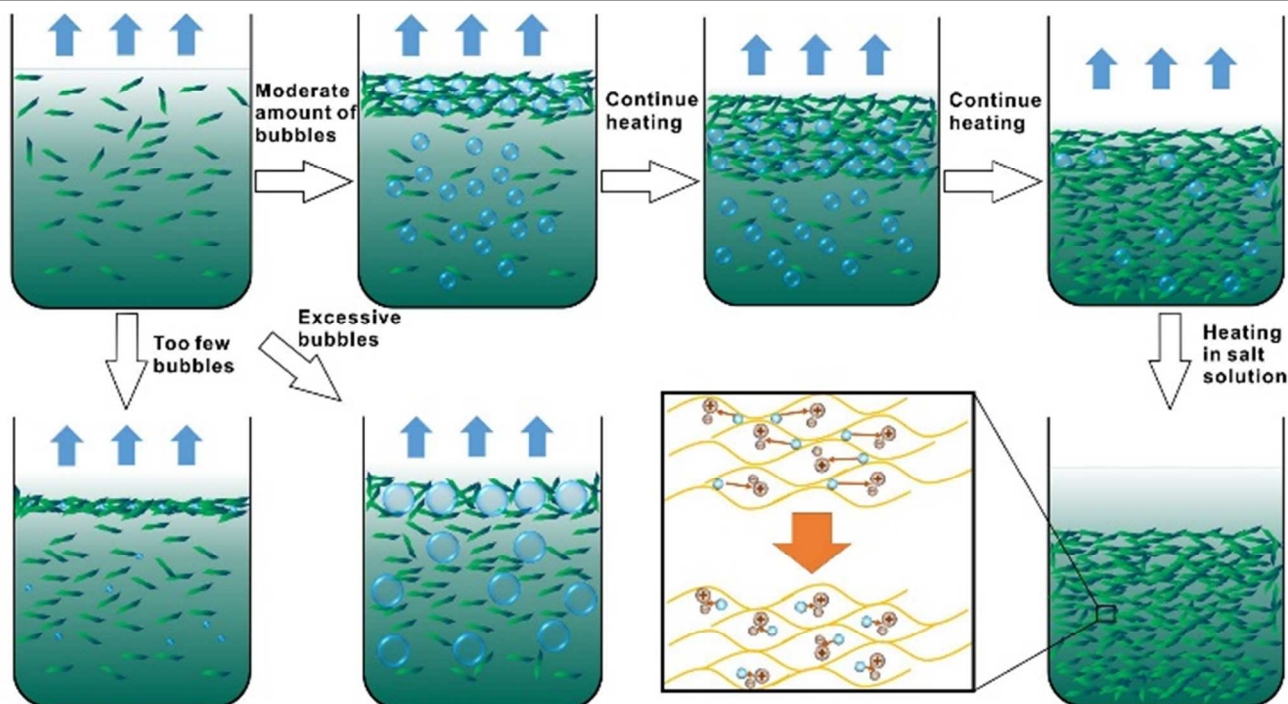| reactant amount	Membrane	Gelation
0.2 g $NaHCO_3$	No	×
0.1 g $NaHCO_3$	Thick	√
0.04 g $NaHCO_3$	Thin	×
0.1 g NH_4HCO_3	No	×
0.05 g NH_4HCO_3	Thick	√
0.02 g NH_4HCO_3	Thin	×
0.1 g $(NH_4)_2CO_3$	No	×
0.05 g $(NH_4)_2CO_3$	Thick	√
0.02 g $(NH_4)_2CO_3$	Thin	×

Fig. 6 Schematic diagrams illustrating the mechanism of hydrogen formation and salt-out effect (the inset).

As a hydrophilic porous material with oxygenated groups, the G-Gel should soak in aqueous solution and interact strongly with transition metal ions. Based on this assumption we investigated the adsorption ability of heavy metals with the G-Gel. As shown in Fig. 7A, a black G-Gel was observed floating on the top after being soaked in a solution of Gold chloride

($HAuCl_4$) and it began to adsorb Au^{3+} ions immediately. After several days, a golden G-Gel was found at the bottom of the vessel and the increase in density could be explained by adsorption and reduction of Au^{3+} ions as the golden color of the solution gradually faded to colorless. (Fig. 7B).

Fig. 7C shows adsorptivity of the G-Gel (prepared with 4 mg mL^{-1} GO) as 63.8 mg g^{-1} for Pt^{4+}, 442.2 mg g^{-1} for Au^{3+}, 301.9 mg g^{-1} for Pb^{2+}, 145.2 mg g^{-1} for Cd^{2+}, 254.4 mg g^{-1} for Ag$^+$ and 73.9 mg g^{-1} for Cu^{2+}, respectively. These values are almost 1~3.5 times high as those of the previous reported rGO aerogel prepared by reduction with mercaptoacetic acid,[39] 2.2~4 times high as the graphene–c-MWCNT hybrid aerogel,[56] 3 times high as the GO aerogel made by freeze-drying,[57] and comparable to polydopamine functionalized graphene hydrogel synthesized using dopamine.[58] These large adsorption capacities with the G-Gel could be ascribed to the existence of large amounts of remaining functional groups due to the incomplete reduction, which is negatively charged and should have strong attractive electrostatic interaction with the positively charged metal ions.[39, 56] The excellent adsorptivity will make the porous G-Gel an ideal candidate as remover of heavy metal ions in practical water purification.
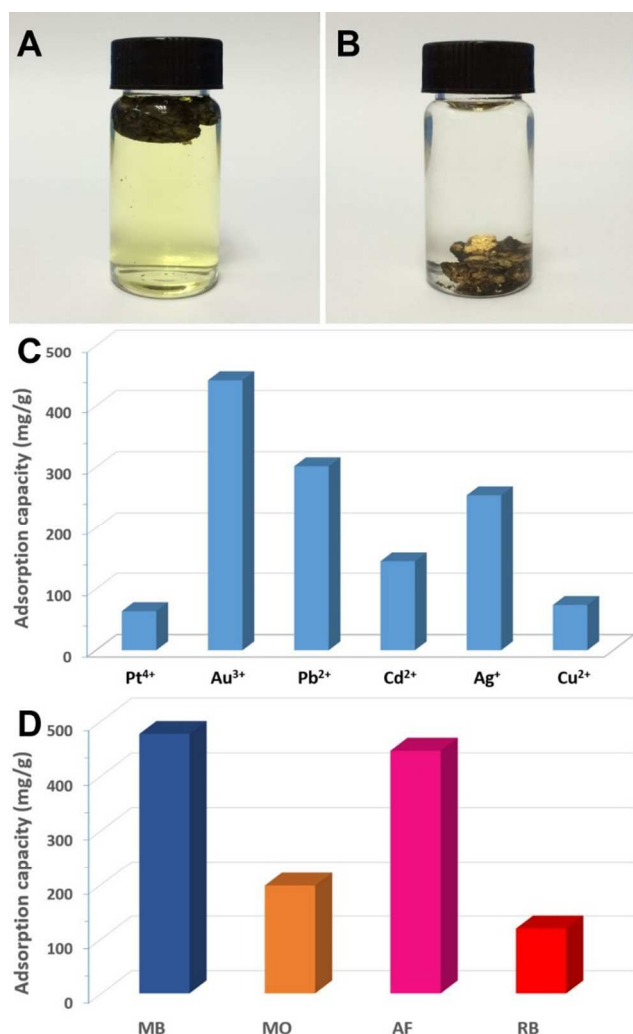

Fig. 7 Photographs of G-Gel after it was soak in HAuCl$_4$ solution in several minutes (A) and several days (B); Adsorption capacities of different heavy metal ions (C) and dyes (D) with G-Gels.

The hydrophilic G-Gel should also have excellent adsorption ability for dyes. Methylene blue (MB), methyl orange (MO), acid fuchsin (AF) and rhodamine B (RB) were used to examine the ability of G-Gel to adsorb dyes from water, and the result is shown in Fig. 7D. The adsorption capacity for MB is 476.1 mg g^{-1}, which is superior to those of most reported materials such as graphene–c-MWCNT hybrid aerogel (190.9 mg g^{-1}),[56] graphene-Cu/Cu$_2$O aerogel fabricated using Cu nanoparticles (140 mg g^{-1}),[59] and micro-mesoporous carbons (10.1-190 mg g^{-1}).[60] The adsorption capacity for MO is 197.6 mg g^{-1}, larger than those of thermally reduced graphene (100 mg g^{-1})[61] and alkali-activated carbon nanotube (149.0 mg g^{-1}),[62] and comparable to graphene-Cu/Cu$_2$O aerogel (250 mg g^{-1}).[59] The adsorption capacity for AF is 445.6 mg g^{-1}, much higher than those of previous reported materials such as carbon–alumina composite pellet (181.82 mg g^{-1})[63] and GO/chitosan fibers (175.4 mg g^{-1}).[64] The adsorption capacity of 118.8 mg g^{-1} for RB is higher than that of 73.0 mg g^{-1} with porous graphitic carbon[65] and 72.5 mg g^{-1} with graphene sponge[66], and comparable to 150 mg g^{-1} with graphene-Cu/Cu$_2$O aerogel,[59] but lower than 207.1 mg g^{-1} with polydopamine functionalized graphene hydrogel.[58] Fig. S2 shows the chemical structure of these dyes. MB and RB are positively charged molecules and should have strong attractive electrostatic interaction with the negatively charged G-Gel. MO and AF are negatively charged and should result in repulsion between G-Gel and the molecules. However, a large amount of MO and AF can still be adsorbed with G-Gel, suggesting that strong π-π interaction between the dyes and G-Gel.[56, 66] Therefore, the adsorption behavior to dyes should be the result of the combined effect of electrostatic and π-π interactions between dyes and G-Gel, but π-π interaction dominated the attraction. Moreover, the adsorbed dyes can be released from G-Gels through immersing the dye-adsorbed G-Gel into ethanol (see Fig. S1, Supplementary Information), reflecting the G-Gel can be regenerated for repeated use. These results suggest that the G-Gel is a hopeful adsorbent for removing dye pollutants from contaminated water.

MB adsorption is a standard method for measuring the specific surface area of graphitic material, since the surface area covered by 1 mg of adsorbed MB is a constant (2.54 m^2). Consequently, the specific surface area (S_S) of G-Gel can be calculated by adsorption of MB with the following equation:[67]

$$S_S \ (m^2 \ g^{-1}) = 2.54 \times M_{MB}/M_{G\text{-}Gel}$$

where M_{MB} (mg) and $M_{G\text{-}Gel}$ (g) are the masses of adsorbed MB and G-Gel, respectively. Based on the above dye adsorption results, the value of $M_{MB}/M_{G\text{-}Gel}$ indicated by the adsorption capacity of the G-Gel to MB is 476.1 mg g^{-1}, thus the specific surface area of G-Gel was calculated to be 1209 m^2 g^{-1}. The large specific surface area of the G-Gel also plays an important role in its adsorption capacity since the aerogel has more surface and charges for metal ion and dye adsorption.

On the other hand, the hydrophobic TG-Gel is highly absorptive for organic solvents (see Fig. S3). This makes it a good candidate for selective superabsorbance. A TG-Gel placed in a water solution with a surface layer of pump oil (dyed with Sudan Black B) rapidly and selectively absorbed the oil and repelled the water (Fig. 8A). Fig. 8B shows the absorption capacities of a TG-Gel prepared with 4 mg mL^{-1} GO for different organic solvents and oils. The absorption capacity characterized by its weight gain is 184 times for toluol, 242 times for chloroform (CF), 222 times for terpineol, 232 times for chlorobenzene (CB), 140 times for cyclohexane (CX), 270 times for polydimethylsiloxane (PDMS), and 230 times for pump oil (PO). These capacities are nearly one order higher than rGO foams prepared by leavening process[33] and graphene-based aerogel fabricated by the reduction of copper nanoparticles,[59] one time higher than rGO foams made by

freeze-drying of GO followed by thermal reduction[68] and graphene sponge assembled with GO sheets by hydrothermal method with the assistance of thiourea,[66] comparable to graphene aerogel obtained by the reacting GO with ethylenediamine,[41] and half that of nitrogen-doped 3D graphene framework prepared by extreme hydrothermal treatment of GO suspension containing pyrrole followed by freeze-drying and annealing at 1050 °C for 3h.[69] In addition, the TG-Gel can be

recovered by simply burning off the absorbed organic liquid without destroying its structure (Fig. 9A). As shown in Fig. 9B, the recovered TG-Gel still keeps its high absorption capability after more than 10 absorption-burning cycles, indicating high recyclability of the TG-Gel. This excellent performance endows the TG-Gel with potential application of removing organics, particularly in the field of oil spills treatment.
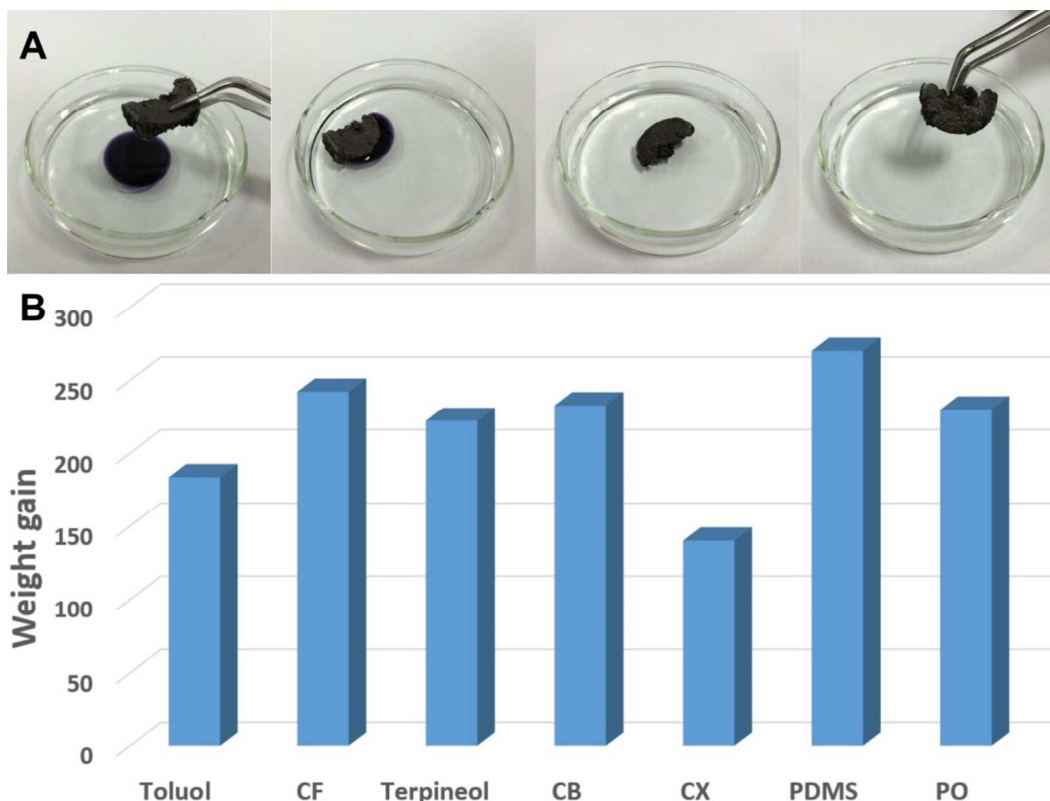

Fig. 8 (A) Absorption process of pump oil (dyed with Sudan Black B) on water by the TG-Gel; (B) Absorption capacities of the TG-Gels for different organic liquids in terms of their weight gain.
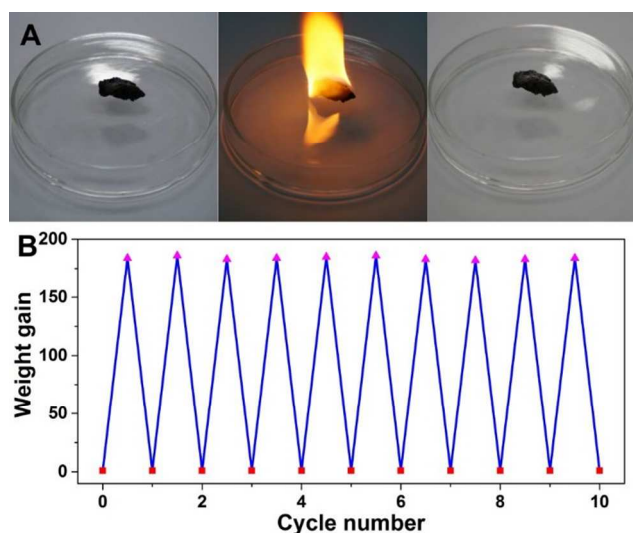

Fig. 9 (A) Photos of a TG-Gel after absorption of toluol (left) and the TG-Gel during (middle) and after (right) burning the absorbed toluol.

(B) Recyclability of the TG-Gel for the absorption of toluol under absorption-burning cycles.

The G-Gel can be deposited on macroporous architectures such as sponges by immersing them into the reaction solution before heating. Fig. 10A shows the photo of various sponges deposited with G-Gels. Owing to sponge as the scaffold, the G-Gel deposited sponge is highly compressible and elastic (Fig. 10B). Combining of high elasticity of sponge and the intrinsic properties of graphene aerogel, it is a possible flexible conductive porous material in many areas.

Fig. 10 Photographs of G-Gel deposited on various sponges (A), and compressibility of the G-Gel deposited sponge (B).

Conclusions

In summary, we developed a green and facile *in situ* reduction-assembly method to prepare graphene hydrogel by heating a mixed solution of GO and $NaHCO_3$. The gelation of reduced graphene oxide can be attributed to that created bubbles prevented the restacking of self-assembled rGO sheets during water evaporation process. The porous G-Gels obtained after freeze-drying of the derived graphene hydrogels exhibit high adsorption capacities to heavy metal ions and dyes. The hydrophobic TG-Gels made by thermal treatment of G-Gels show great performance as recyclable selective absorbents for organic liquids. The ease of preparation and excellent performance could endow porous G-Gels and TG-Gels with promising application as environmental remediation materials. In addition, these porous aerogels can be further exploited for various other applications, such as energy storage, catalyst supports, and sensors and so on.

## Acknowledgements

Notes and references

[a]Hefei National Laboratory for Physical Sciences at Microscale, and Department of Physics, University of Science and Technology of China, Hefei, Anhui, 230026, P. R. China. E-mail: zhuw@ustc.edu.cn (W. Zhu), gzwang@ustc.edu.cn (G. Wang). Tel.: +86 551 63603323; fax: +86 551 63606266

[b]School of Material Science and Engineering, North University of Nationalities, Yinchuan, Ningxia, 750021, P. R. China

1. K. S. Novoselov, A. K. Geim, S. V. Morozov, D. Jiang, Y. Zhang, S. V. Dubonos, I. V. Grigorieva and A. A. Firsov, *Science*, 2004, **306**, 666-669.
2. A. K. Geim and K. S. Novoselov, *Nat. Mater.*, 2007, **6**, 183-191.
3. A. H. Castro Neto, F. Guinea, N. M. R. Peres, K. S. Novoselov and A. K. Geim, *Rev. Mod. Phys.*, 2009, **81**, 109-162.
4. C. N. R. Rao, A. K. Sood, K. S. Subrahmanyam and A. Govindaraj, *Angew. Chem. Int. Ed.*, 2009, **48**, 7752-7777.
5. M. J. Allen, V. C. Tung and R. B. Kaner, *Chem. Rev.*, 2010, **110**, 132-145.
6. D. Chen, L. H. Tang and J. H. Li, *Chem. Soc. Rev.*, 2010, **39**, 3157-3180.
7. C. K. Chua and M. Pumera, *Chem. Soc. Rev.*, 2014, **43**, 291-312.
8. F. J. G. de Abajo, *Acs Photonics*, 2014, **1**, 135-152.
9. D. Zhan, J. X. Yan, L. F. Lai, Z. H. Ni, L. Liu and Z. X. Shen, *Adv. Mater.*, 2012, **24**, 4055-4069.
10. D. C. Wei, B. Wu, Y. L. Guo, G. Yu and Y. Q. Liu, *Acc. Chem. Res.*, 2013, **46**, 106-115.
11. Q. L. Bao and K. P. Loh, *Acs Nano*, 2012, **6**, 3677-3694.
12. F. Bonaccorso, Z. Sun, T. Hasan and A. C. Ferrari, *Nat. Photonics*, 2010, **4**, 611-622.
13. J. Liu, M. Durstock and L. M. Dai, *Energy Environ. Sci.*, 2014, **7**, 1297-1306.
14. S. Han, D. Q. Wu, S. Li, F. Zhang and X. L. Feng, *Adv. Mater.*, 2014, **26**, 849-864.
15. G. Z. Kyzas, E. A. Deliyanni and K. A. Matis, *J. Chem. Technol. Biotechnol.*, 2014, **89**, 196-205.
16. X. K. Kong, C. L. Chen and Q. W. Chen, *Chem. Soc. Rev.*, 2014, **43**, 2841-2857.
17. S. L. Yang, Y. W. Huang, W. Zhu, B. C. Deng, H. Wang, Z. H. Zhang, P. F. Bao and G. Z. Wang, *Int. J. Hydrogen Energy*, 2014, **39**, 15063-15071.
18. Q. Y. He, S. X. Wu, Z. Y. Yin and H. Zhang, *Chem. Sci.*, 2012, **3**, 1764-1772.
19. F. Yan, M. Zhang and J. H. Li, *Adv. Healthcare Mater.*, 2014, **3**, 313-331.
20. L. Zhang, J. T. Wu and L. Jiang, *Prog. Chem.*, 2014, **26**, 560-571.
21. M. Yang, J. Yao and Y. X. Duan, *Analyst*, 2013, **138**, 72-86.
22. A. P. Pandey, K. P. Karande, M. P. More, S. G. Gattani and P. K. Deshmukh, *J. Biomed. Nanotechnol.*, 2014, **10**, 179-204.
23. L. L. Jiang and Z. J. Fan, *Nanoscale*, 2014, **6**, 1922-1945.
24. S. Nardecchia, D. Carriazo, M. L. Ferrer, M. C. Gutierrez and F. del Monte, *Chem. Soc. Rev.*, 2013, **42**, 794-830.
25. C. Li and G. Q. Shi, *Nanoscale*, 2012, **4**, 5549-5563.
26. Z. F. Zhao, X. B. Wang, J. L. Qiu, J. J. Lin, D. D. Xu, C. Zhang, M. J. Lv and X. Y. Yang, *Rev. Adv. Mater. Sci.*, 2014, **36**, 137-151.
27. V. Chabot, D. Higgins, A. P. Yu, X. C. Xiao, Z. W. Chen and J. J. Zhang, *Energy Environ. Sci.*, 2014, **7**, 1564-1596.
28. S. Yin, Y. Zhang, J. Kong, C. Zou, C. M. Li, X. Lu, J. Ma, F. Y. C. Boey and X. Chen, *ACS Nano*, 2011, **5**, 3831-3838.

29. S. H. Lee, H. W. Kim, J. O. Hwang, W. J. Lee, J. Kwon, C. W. Bielawski, R. S. Ruoff and S. O. Kim, *Angew. Chem. Int. Ed.*, 2010, **49**, 10084-10088.

30. X. D. Huang, K. Qian, J. Yang, J. Zhang, L. Li, C. Z. Yu and D. Y. Zhao, *Adv. Mater.*, 2012, **24**, 4419-4423.

31. Z. Chen, W. Ren, L. Gao, B. Liu, S. Pei and H.-M. Cheng, *Nat Mater*, 2011, **10**, 424-428.

32. W. Chen, Z. L. Fan, G. F. Zeng and Z. P. Lai, *J. Power Sources*, 2013, **225**, 251-256.

33. Z. Q. Niu, J. Chen, H. H. Hng, J. Ma and X. D. Chen, *Adv. Mater.*, 2012, **24**, 4144-4150.

34. X. W. Yang, L. Qiu, C. Cheng, Y. Z. Wu, Z. F. Ma and D. Li, *Angew. Chem. Int. Ed.*, 2011, **50**, 7325-7328.

35. M. A. Worsley, P. J. Pauzauskie, T. Y. Olson, J. Biener, J. H. Satcher and T. F. Baumann, *J. Am. Chem. Soc.*, 2010, **132**, 14067-14069.

36. V. H. Luan, H. N. Tien, L. T. Hoa, T. M. H. Nguyen, E. S. Oh, J. Chung, E. J. Kim, W. M. Choi, B. S. Kong and S. H. Hur, *J. Mater. Chem. A*, 2013, **1**, 208-211.

37. H. Bai, C. Li, X. L. Wang and G. Q. Shi, *J. Phys. Chem. C*, 2011, **115**, 5545-5551.

38. L. B. Zhang, G. Y. Chen, M. N. Hedhili, H. N. Zhang and P. Wang, *Nanoscale*, 2012, **4**, 7038-7045.

39. M. Chen, C. Zhang, X. Li, L. Zhang, Y. Ma, L. Zhang, X. Xu, F. Xia, W. Wang and J. Gao, *J. Mater. Chem. A*, 2013, **1**, 2869-2877.

40. Y. X. Xu, K. X. Sheng, C. Li and G. Q. Shi, *Acs Nano*, 2010, **4**, 4324-4330.

41. J. H. Li, J. Y. Li, H. Meng, S. Y. Xie, B. W. Zhang, L. F. Li, H. J. Ma, J. Y. Zhang and M. Yu, *J. Mater. Chem. A*, 2014, **2**, 2934-2941.

42. X. Z. Wu, J. Zhou, W. Xing, G. Q. Wang, H. Y. Cui, S. P. Zhuo, Q. Z. Xue, Z. F. Yan and S. Z. Qiao, *J. Mater. Chem.*, 2012, **22**, 23186-23193.

43. S. Pei, J. Zhao, J. Du, W. Ren and H.-M. Cheng, *Carbon*, 2010, **48**, 4466-4474.

44. H. D. Pham, V. H. Pham, T. V. Cuong, T. D. Nguyen-Phan, J. S. Chung, E. W. Shin and S. Kim, *Chem. Commun.*, 2011, **47**, 9672-9674.

45. W. F. Chen and L. F. Yan, *Nanoscale*, 2011, **3**, 3132-3137.

46. Y. X. Xu, Z. Y. Lin, X. Q. Huang, Y. Wang, Y. Huang and X. F. Duan, *Adv. Mater.*, 2013, **25**, 5779-+.

47. J. F. Liang, Z. Cai, L. D. Li, L. Guo and J. X. Geng, *RSC Adv.*, 2014, **4**, 4843-4847.

48. W. S. Hummers and R. E. Offeman, *J. Am. Chem. Soc.*, 1958, **80**, 1269-1522.

49. S. Stankovich, D. A. Dikin, R. D. Piner, K. A. Kohlhaas, A. Kleinhammes, Y. Jia, Y. Wu, S. T. Nguyen and R. S. Ruoff, *Carbon*, 2007, **45**, 1558-1565.

50. D. R. Dreyer, S. Park, C. W. Bielawski and R. S. Ruoff, *Chem. Soc. Rev.*, 2010, **39**, 228-240.

51. C. Zhu, S. Guo, Y. Fang and S. Dong, *Acs Nano*, 2010, **4**, 2429-2437.

52. S. Dubin, S. Gilje, K. Wang, V. C. Tung, K. Cha, A. S. Hall, J. Farrar, R. Varshneya, Y. Yang and R. B. Kaner, *Acs Nano*, 2010, **4**, 3845-3852.

53. T. N. Zhou, F. Chen, K. Liu, H. Deng, Q. Zhang, J. W. Feng and Q. A. Fu, *Nanotechnology*, 2011, **22**, 6.

54. Y. Wang, P. Zhang, C. F. Liu and C. Z. Huang, *RSC Adv.*, 2013, **3**, 9240-9246.

55. X. B. Fan, W. C. Peng, Y. Li, X. Y. Li, S. L. Wang, G. L. Zhang and F. B. Zhang, *Adv. Mater.*, 2008, **20**, 4490-4493.

56. Z. Sui, Q. Meng, X. Zhang, R. Ma and B. Cao, *J. Mater. Chem.*, 2012, **22**, 8767-8771.

57. X. Mi, G. B. Huang, W. S. Xie, W. Wang, Y. Liu and J. P. Gao, *Carbon*, 2012, **50**, 4856-4864.

58. H. C. Gao, Y. M. Sun, J. J. Zhou, R. Xu and H. W. Duan, *ACS Appl. Mater. Interfaces*, 2013, **5**, 425-432.

59. T. Wu, M. Chen, L. Zhang, X. Xu, Y. Liu, J. Yan, W. Wang and J. Gao, *J. Mater. Chem. A*, 2013, **1**, 7612-7621.

60. B. S. Girgis, A. M. Soliman and N. A. Fathy, *Microporous Mesoporous Mater.*, 2011, **142**, 518-525.

61. M. Z. Iqbal and A. A. Abdala, *RSC Adv.*, 2013, **3**, 24455-24464.

62. J. Ma, F. Yu, L. Zhou, L. Jin, M. Yang, J. Luan, Y. Tang, H. Fan, Z. Yuan and J. Chen, *ACS Appl. Mater. Interfaces*, 2012, **4**, 5749-5760.

63. M. Dutta and J. K. Basu, *Int. J. Environ. Sci. Technol.*, 2014, **11**, 87-96.

64. Y. Li, J. Sun, Q. Du, L. Zhang, X. Yang, S. Wu, Y. Xia, Z. Wang, L. Xia and A. Cao, *Carbohydr. Polym.*, 2014, **102**, 755-761.

65. L. Sun, C. Tian, L. Wang, J. Zou, G. Mu and H. Fu, *J. Mater. Chem.*, 2011, **21**, 7232-7239.

66. J. Zhao, W. Ren and H.-M. Cheng, *J. Mater. Chem.*, 2012, **22**, 20197-20202.

67. M. J. McAllister, J. L. Li, D. H. Adamson, H. C. Schniepp, A. A. Abdala, J. Liu, M. Herrera-Alonso, D. L. Milius, R. Car, R. K. Prud'homme and I. A. Aksay, *Chem. Mater.*, 2007, **19**, 4396-4404.

68. Y. Q. He, Y. Liu, T. Wu, J. K. Ma, X. R. Wang, Q. J. Gong, W. N. Kong, F. B. Xing, Y. Liu and J. P. Gao, *J. Hazard. Mater.*, 2013, **260**, 796-805.

69. Y. Zhao, C. Hu, Y. Hu, H. Cheng, G. Shi and L. Qu, *Angew. Chem. Int. Ed.*, 2012, **51**, 11371-11375.
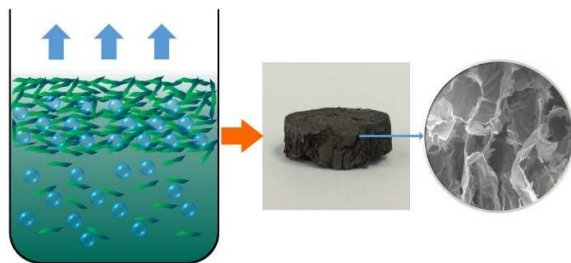
We present a new type of *in situ* reduction-assembly approach to construct graphene hydrogel through simultaneous water evaporation and graphene oxide reduction.